Thermal Properties of Optomechanical Photonic Crystals

Author: Xuanhao Qiu.
*Facultat de Física, Universitat de Barcelona, Diagonal 645, 08028 Barcelona, Spain.**

Advisor: Daniel Navarro Urrios

Abstract: In many fields such as electronics or photonics, thermal effects play a significant role in the overall functioning of the devices. Therefore, it is important to understand and quantify their impact. In this work, we study these effects in a specific type of photonic device, namely a one-dimensional photonic crystal, which is at the same time a collection of mechanical resonators. Specifically, we investigated the dominant dissipation mechanism in nanopillars heated by the electromagnetic field, considering 2 different types of nanopillars: the full silicon cell (FSC) and SiO_2 cell (SiO_2C). Initially, we obtained the optical modes to acquire the spatial electric field distribution to use as the heat source in the nanopillars. The first study involved heating with the electric field distribution at 195.96 THz. The decay rates obtained were: $1/\tau_{Si} = 7.67$ MHz and $1/\tau_{SiO_2} = 2.22$ MHz. Subsequently, we studied the decay rates as the radius of the structures decreased. For FSC, the decay rate decreased, whereas for SiO_2C, it increased. Aditionally, we calculated the dissipation process for another electric field distribution (230.99 THz). The decay rates obtained were slightly lower than the first study, $1/\tau'_{Si} = 7.40$ MHz and $1/\tau'_{SiO_2} = 1.99$ MHz. Finally, we compared the values from the first study to experimental values. The experimental value for FSC was 29.63% higher, while for SiO_2C, the simulated value was 9.90% higher. We concluded that the dominant dissipation mechanism for FSC is conduction due to dissipation through the bottom silicon pillar. In contrast, for SiO_2C, the dominant dissipation mechanism is convection, as thermal transport through the bottom SiO_2 pillar is negligible.

I. INTRODUCTION

Optomechanical crystals are periodic structures that enable control over both light and phonons [1]. They have garnered significant research interest in recent years due to their potential applications in light modulation [2], quantum processing [3] or biosensors [4-5].

From a properly designed structure, it is possible to create a band diagram featuring an energy gap for both photonic and phononic components. This enables the confinement of optical and mechanical modes, forming the optomechanical cavity [6].

The structures examined in this work are 1D photonic crystal composed of nanopillars, as illustrated in **Figure 1**. These structures are employed as a highly sensitive force sensor due to their exceptional mechanical properties [4].

The first one is illustrated in **Figure 1a** and is composed entirely of silicon, with the radius of the bottom pillar being $\Delta r = 50$ nm smaller than that of the top pillar. In **Figure 1b**, where the top pillar is made of silicon and the bottom pillar is made of SiO_2, both having the same radius. To create a cavity, the pillars' radius is reduced quadratically towards the center [6].

The objective of this investigation is to study the dominant heat dissipation processes due to electromagnetic heating in these nanopillar structures. Understanding heat dissipation is crucial because experiments have shown that temperature increases in the pillars can alter

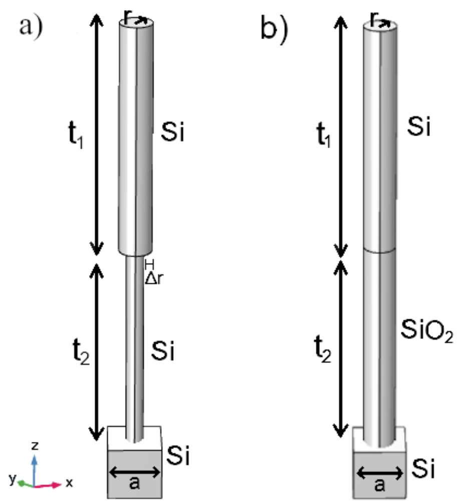

Figure 1: a) Nanopillar made entirely of silicion with the following parameter values: $t_1 = t_2 = 1500$ nm, $a = 350$ nm, $r = 105$ nm and $\Delta r = 50$ nm. b) Nanopillar with a top pillar made of silicion and a bottom pillar made of SiO_2 (both having the same radius) with the following parameter values: $t_1 = t_2 = 1500$ nm, $a = 350$ nm and $r = 105$ nm.

the frequencies of certain mechanical and optical modes [6-7]. The alteration is attributed to variations in the refractive index, the elastic constants and/or material expansion, which are temperature dependent. Additionally, the decay rate provides us with an idea of how long the system would take to dissipate the heat (characteristic time).

*Electronic address: xqiuqiux7@alumnes.ub.edu

Even though the energy of the photons is below the gap energy of silicon, a fraction of the light stored in the cavity is absorbed by single photon absorption. This is a consequence of the presence of many intragap states present in the surface of the silicon geometries so that single photon light abosption can excite free carriers into the valence or conduction bands. The energy excess of these free carriers can be released by means non radiative processes, which lead into the heating of these geometries.

To analyse the dominant heat dissipation mechanism, we will heat the structures from **Figure 1** with a normalized electric field extracted from a specific optical mode. Once the structure arrives to a stationary mode, we will turn off the heat source and observe the thermal decay. We will repeat this process for different sizes and examine how the decay rates vary. To make this study more comprehensible and easier, only the cases where the optical mode is confined in the top pillar are considered.

II. METHODS

For the entire study, we used COMSOL Multiphysics to simulate both the optical and thermal parts. This multiphysics simulation software allows us to obtain both optical modes and analyze the thermal dissipation processes.

The primary aim of this investigation is to determine how to use the electric field distribution from a specific optical mode as the heat source. Then, the dissipation process will be observed by turning off the heat source after defining boundary conditions on the substrate and the air as ambient temperature. Consequently, the initial study will focus on the optical aspects, and after obtaining the optical modes, the heat study will be conducted.

It is important to mention that this study will be conducted using a single unit cell, as illustrated in **Figure 1**, rather than the entire periodic structure. Therefore, we assume that the effects of thermal transfer between neighboring unit cells in the periodic structure are negligible, as the cells are sufficiently far apart to prevent interaction between them.

III. EQUATIONS

As this investigation is centered on heat transfer in nanopillars, the analysis will primarily focus on the "Heat Transfer Module" from COMSOL Multiphysics. From the software documentation, the heat transfer is modeled as follows [8]:

$$\rho C_p \frac{\partial T}{\partial t} + \rho C_p u \nabla T + \nabla q = Q + Q_{ted} \tag{1}$$

$$q = -k \nabla T \tag{2}$$

$$Q_{ted} = -\alpha T \frac{dS}{dt} \tag{3}$$

Where ρ is the density, C_p is the specific heat capacity, T is the absolute temperature, u is the translational motion velocity vector, q is the conduction heat flux, k is the material heat conductivity, Q is the additional heat sources, Q_{ted} is the thermoelastic damping (heat source caused by compression or expasion of the solid), S is the second Piola-Kirchhoff stress tensor (relates the force to areas on the configuration), α is the thermal expansion coefficient and $\frac{\partial T}{\partial t}$ represents the evolution of temperature field. In our case, the values of Q will be the normalized electric field.

IV. DEVELOPING SECTIONS

As mentioned previously, two studies have been conducted: one focusing on optical aspects and the other on thermal analysis.

A. Optical modes

The optical study has only been conducted for the structure in **Figure 1a**, as the optical modes for the other structure are nearly identical. Indeed, the frequency and spatial distrbution of the optical mode are dominated by the geometrical configuration of the upper region of the nanopillars, which is the same for both cases under study.

The unit cell is artificially repeated by imposing periodic boundary conditions, with a separation distance a between each identical cell units along the x-axis. Therefore, we can obtain the optical band diagram displayed in **Figure 2**. The results are obtained for the Transverse Magnetic (TM) optically polarized mode, as there are no Transverse Electric polarized optical modes supported by these geometries. The parameters used were $a = 350$ nm, $r = 105$ nm and $t_1 = t_2 = 1500$ nm. We can observe that the center of the energy bandgap for this configuration is located around 200 THz. This is a correct location since our lasers are tuneable between 1355–1640 nm or 182-221 THz. The electric fields located at the point $kx = \frac{\pi}{a}$ are distributed an the top of the pillar, as shown in **Figure 3**.

The right side of **Figure 2** illustrates the frequency variation at the X-point of the band diagram when changing the size of the pillars a factor f for the both pillar radius, while keeping the same height and Δr. This gives us an intuition on how to modify the geometry so that it is possible to create a defect by placing a resonant optical mode within the energy bandgap. To construct the nanopillar cavity, we will position two mirrors consisting of 9 cells each with the initial size (having the band diagram of **Figure 2**). We will introduce to the defect zone 11 cells, and the radius of the cells will be reduced quadratically towards the center, with a minimum value as f*r. The cavity is shown in the **Figure 7**, since this work is not focused on this topic, no simulations regarding this nanopillars cavity have been performed.

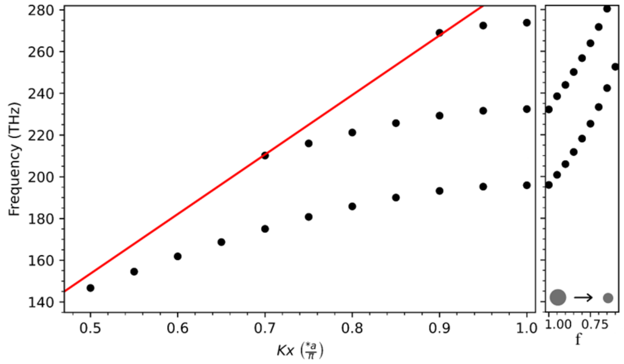

Figure 2: Optical modes band diagram. The light line is depicted in red. The graph on the right shows the edge frequency variation as the radius of pillars decreases.

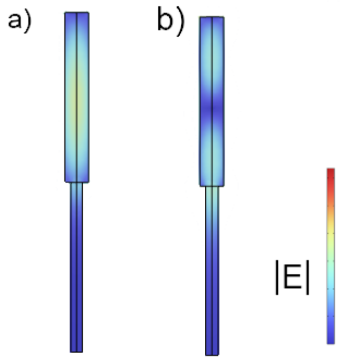

Figure 3: a) Normalized spatial electric field distribution for the frequency of 195.96 THz. b) Normalized spatial electric field distribution for the frequency of 230.99 THz. Both solutions correspond to $k_x = \frac{\pi}{a}$, i.e., the edge of the first Brillouin zone.

B. Thermal simulation

Having obtained the spatial distribution of the electric field in the preceding section, we can now integrate it with the thermal part.

Firstly, we extracted the electric field spatial distribution values from COMSOL. Then, a modification process for these values was executed in Python. Specifically, we calculated the modulus of the electric field values as we do not want negative heating sources. Then, we normalized the values by dividing them by the maximum value. Finally, these values were multiplied by a factor 10000 to ensure a reasonable increase in temperature for the heat source. This factor is not relevant, as the decay rate would remain unaffected by an alteration in its value.

Once the heat source values are obtained, we could study both the heating and dissipation processes. However, the dissipation process provides directly the dissipation rate, and thus has been the primary focus of this investigation.

The first study was executed for the pillars with the original size (f=1), heating them with the electric field distribution of 195.96 THz, shown in **Figure3a**. We heated the pillars until they reached a stationary mode, corresponding to the situation depicted in **Figure 4b** and **Figure 5b**. After that, the heating sources were deleted, and natural dissipation started. If we are located at the point X in **Figure 4b** and **Figure 5b**, we can obtain the values of temperature as a function of time from COMSOL Multiphysics. This variation is shown in **Figure 4a** and **Figure 5a**. According to the graphs, it's evident that they exhibit an exponential decay behavior, so an exponential regression was performed in Python.

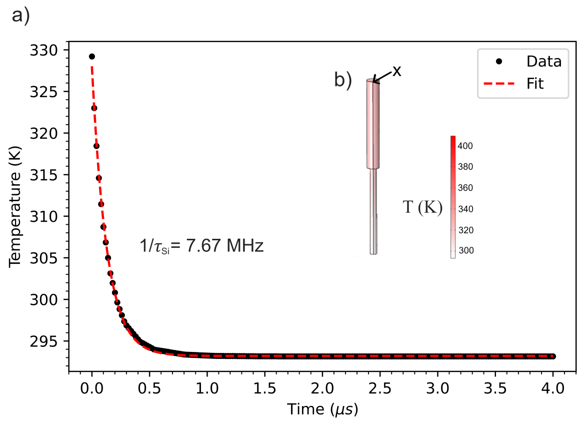

Figure 4: a) The temperature as a function of time at the point X. It shows an exponential regression with following equation: $T(t) = 38.59e^{-7.67t}+293.24$. b) Spatial distribution of the temperature when the thermal stationary mode of the FSC is reached, heated by the electric field distribution from **Figure 3a**.

From the regressions, we obtained a decay rate for FSC of $1/\tau_{Si} = 7.67$ MHz and $1/\tau_{SiO_2} = 2.22$ MHz for SiO_2C. It is interesting to note that the decay rate of FSC is higher than SiO_2C, suggesting that the main dissipation mechanism for FSC is conduction through the bottom silicon pillar. Unlike the SiO_2 pillar, which is a poor thermal conductor and does not exhibit an elevated conduction effect, resulting in a lower decay rate. Thus, in this case, dissipation primarily occurs through convection.

In the next study, we will vary the radius of the top and bottom pillars with the factor f, as conduction highly depends on the area. We conducted a study by decreasing f by 0.05 from 1 to 0.6. The electric fields distribution are calculed for each size, since the spatial distribution is slighly different for each size. It is worth noting that, when performing the rescaling of the FSC radius, Δr is

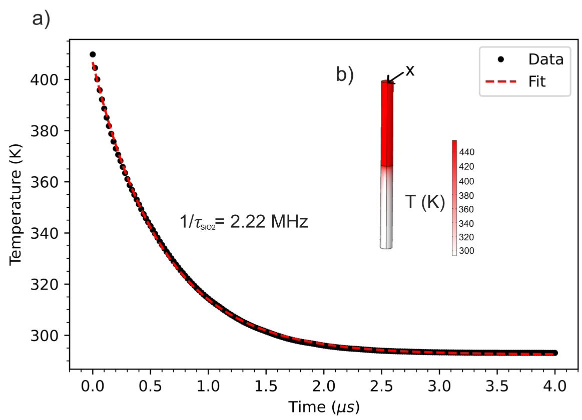

Figure 5: a) The temperature as a function of time at the point X. It shows an exponential regression with following equation: $T(t) = 129.49e^{-2.22t} + 292.92$. b) Spatial distribution of the temperature when the thermal stationary mode of SiO_2C is reached, heated by the electric field distribution from Figure 3a.

kept to be 50 nm in accordance to restrictions in the fabricated devices. The decay rates are shown in **Figure 6**.

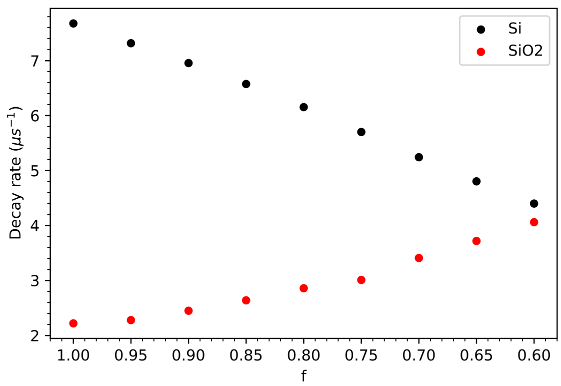

Figure 6: Decay rates as function of the factor f. Red points corresponding to SiO_2C and black points corresponding to FSC.

When the radius of the pillars reduces, in FSC, the decay rates decrease due to the reduced conduction area through the bottom pillar. Hence, we observe a decrease in the decay rate with each reduction in area. In contrast, in SiO_2C, the decay rates increase is attributed to a higher convection, as there is no significant thermal conduction through the bottom pillar due to SiO_2 low thermal conductivity. This provides further evidence that in FSC, the dominant heat dissipation mechanism is conduction, while for the other case, it is convection. **Figure 6** also shows that both curves seem to tend to similar thermal dissipation rate values, indicating that they converge to be dominated by the same mechanism, i.e. convection. This is an expected result since, in the FSC case, we are eliminating the conduction channel through the bottom part of the pillar and only convection in the top part of the pillar remains. Given that conduction through the bottom portion of the pillar is negligible for the SiO2C case, both types of pillars become almost equivalent when f is low enough.

Finally, we calculated the heat dissipation for another electric field distribution, as illustrated in **Figure 3b**. The decay rate obtained for the FSC is $1/\tau'_{Si} = 7.40$ MHz, and for the SiO_2C, it is $1/\tau'_{SiO_2} = 1.99$ MHZ. We can observe that the decay rates are slightly lower than in the previous study, as the heating effects of this electric field are weaker. Indeed, the heating and dissipation processes at 230.99 THz are similar to those at 195.96 THz, as evidenced by the similarity in the temperature-time graphs.

C. Comparison with experimental values

The experiment consisted to calculate the decay rate for the periodic structure of nanopillars made by silicon and SiO_2 with the Bode diagram, as shown in **Figure 8**.

The experiment involves the utilization of two lasers, resonant with two optical modes. One laser is optically modulated at various frequencies, while the other is employed for transmission detection. As the modulation of the laser changes, the frequency of the optical modes is altered due to the temperature increase. Consequently, the detection laser captures a variation of transmission, enabling the creation of the Bode diagram, illustrating transmission as a function of frequency. These experimental values are provided by Dr. Daniel Navarro.

For the full silicon structure the experimental decay rate is $1/\tau^{exp}_{Si} = 11$ MHz. Comparing with simulated results, $1/\tau^{sim}_{Si} = 7.67$ MHz $< 1/\tau^{exp}_{Si} = 11$ MHz. The experimental value is 29.63% higher, possibly because the simulation assumes perfect conditions. Besides, in the real structure, the radius of the bottom pillar may be slightly larger than in the simulated one, as illustrated in **Figure7**.

For the SiO_2 structure the experimental decay rate is $1/\tau^{exp}_{SiO_2} = 2$ MHz. Comparing with simulated results, $1/\tau^{sim}_{SiO_2} = 2.22$ MHz $< 1/\tau^{exp}_{SiO_2} = 2$ MHz. In this case, both results are quite similar (the simulated value is 9.90% higher) since in this structure, the dominant dissipation mechanism is convection, and the dependence on the area is not as significant as in the full silicon structure.

V. CONCLUSIONS

In this work, we investigated the dissipation process caused by electromagnetic heating in 2 structures: full silicon cell and SiO_2 cell. The decay rate obtained for

FSC is higher than SiO_2C due to the conduction through the bottom pillar. Besides, conduction is the dominant dissipation mechanism in FSC, while in SiO_2C is convection.

Furthermore, we also calculated the decay rates for the electric field distribution located in 230.99 THz. The values obtained from this distribution were minimally lower than the electric field distribution of 195.96 THz.

We also compared the decay rate with experimental values. In FSC, the experimental value is higher than the simulated value due to imperfections in the real structure. In SiO_2C, the both values values are similar. Hence, this simulation can offer us valuable insights into the behavior of the real structure.

In conclusion, it is crucial to consider the thermal effects in nanopillars when studying these structures. For future investigations, it would be interesting to develop structures that minimize the heating effect by selecting a less heating electric field to create the cavity or by modifying the structure to enhance thermal dissipation.

VI. APPENDIX

The nanopillars photonic crystal cavity is shown in **Figure 7**. Although it is not the main focus of this study, it is relevant to compare and observe the real structures alongside the simulated ones. We can clearly observe that the bottom pillars in **Figure7e** are larger than in the simulation, leading to an increase in thermal conduction through that region.

The Bode diagram is illustrated in **Figure 8**. The experimental values of decay rates are obtained as the transmission drops by -3 dB. The frequency at which this decay occurs is considered the experimental characteristic time.

Acknowledgments

I would like to thank my advisor, Dr. Daniel Navarro, for his guidance and provision of resources throughout this work. Additionally, I would like to express my gratitude to my family and friends for their unwavering support and encouragement.

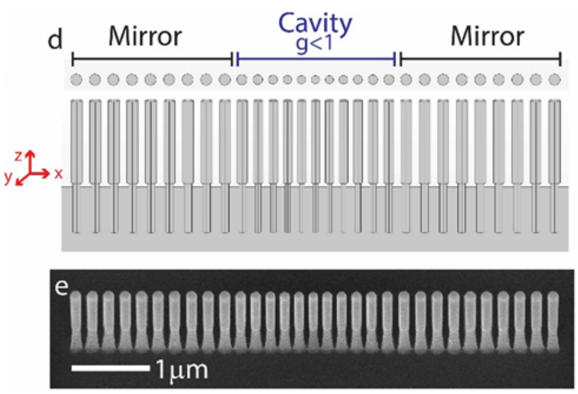

Figure 7: d) Illustration of nanopillars photonic crystal cavity in COMSOL. e) Illustration of the nanopillars cavity scanned by electron microscope. The radius of the center pillar is reduced by $g = 0.75$

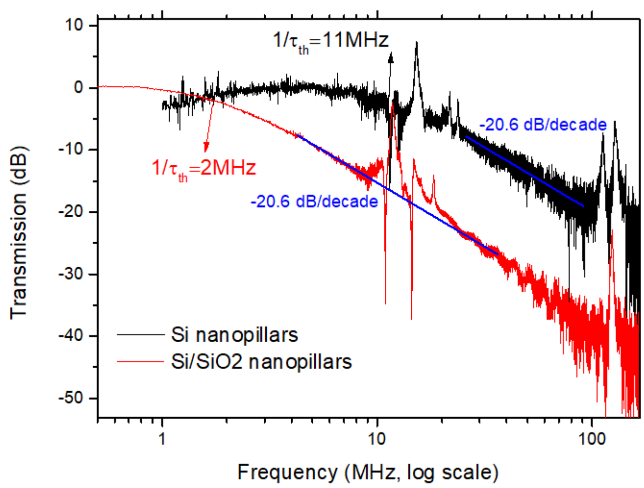

Figure 8: Transmission as a function of frequency (in log scale). Red values represent SiO_2 nanopillars and black values represent Si nanopillars. The decay rates obtained are $1/\tau^{exp}_{SiO_2} = 2$ MHz and $1/\tau^{exp}_{Si} = 11$ MHz. It also includes the slope for both materials, which is -20.6 dB/decade.

[1] Oudich, M. et al. "Optomechanic interaction in a corrugated phoxonic nanobeam cavity." Physical Review B **89**, 245122 (2014).
[2] Zhang, Y. et al. "Photonic crystal nanobeam lasers." Applied Physics Letters **97**. 10.1063/1.3475397. (2010).
[3] Ellis, B. et al. "Ultralow-threshold electrically pumped quantum-dot photonic-crystal nanocavity laser." Nat Photonics 10.1038. (2011).
[4] Jaramillo-Fernandez, J. et al. "Full Silicon Pillar-based 1D Optomechanical cavities." arXiv:2405.18319. (2024).
[5] Pitruzzello, G. Krauss, T. F. "Photonic crystal resonances for sensing and imaging." Journal of Optics **20**, 073004 (2018).
[6] J. Chan, H. Safavi-Naeini, T. Hill, S. Meenehan, O. Painter. "Optimized optomechanical crystal cavity with acoustic radiation shield." arXiv:1206.2099. (2012).
[7] M. W. Lee, et al. "Photosensitive and thermal nonlinear effects in chalcogenide photonic crystal cavities," Opt. Express **18**, 26695-26703 (2010).
[8] "doc.comsol.com" COMSOL. (2018). "Heat Transfer Module User's Guide"